Molecular Dynamics Study of Water and Na$^+$ Ions in Models of the Pore Region of the Nicotinic Acetylcholine Receptor

G. R. Smith and M. S. P. Sansom

Laboratory of Molecular Biophysics, University of Oxford, Oxford OX1 3QU, England

ABSTRACT The nicotinic acetylcholine receptor (nAChR) is an integral membrane protein that forms ligand-gated and cation-selective channels. The central pore is lined by a bundle of five approximately parallel M2 helices, one from each subunit. Candidate model structures of the solvated pore region of a homopentameric $(\alpha 7)_5$ nAChR channel in the open state, and in two possible forms of the closed state, have been studied using molecular dynamics simulations with restraining potentials. It is found that the mobility of the water is substantially lower within the pore than in bulk, and the water molecules become aligned with the M2 helix dipoles. Hydrogen-bonding patterns in the pore, especially around pore-lining charged and hydrophilic residues, and around exposed regions of the helix backbone, have been determined. Initial studies of systems containing both water and sodium ions together within the pore region have also been conducted. A sodium ion has been introduced into the solvated models at various points along the pore axis and its energy profile evaluated. It is found that the ion causes only a local perturbation of the water structure. The results of these calculations have been used to examine the effectiveness of the central ring of leucines as a component of a gate in the closed-channel model.

INTRODUCTION

The nicotinic acetylcholine receptor (nAChR) is the best-understood member of the ligand-gated ion channel superfamily (Stroud et al., 1990; Galzi et al., 1992; Lester, 1992; Karlin and Akabas, 1995; Hucho et al., 1996). In muscle, nAChRs mediate fast signal transmission from nerve end plate to muscle fiber, whereas the function of neuronal nAChRs is less clear and may be mainly modulatory (Role and Berg, 1996). nAChRs are also found in the electric organ of the electric ray *Torpedo* (where they resemble those found in muscle).

The nAChR has a pentameric stoichiometry and forms cation-selective channels. Hydropathy analysis suggests that each subunit has four hydrophobic segments, known as M1–M4. Photolabeling experiments with open-channel blockers (Hucho et al., 1986; Giraudat et al., 1987) and site-directed mutagenesis experiments (Imoto et al., 1988; Leonard et al., 1988; Charnet et al., 1990; Villarroel et al., 1991; Cohen et al., 1992; Akabas et al., 1992, 1994) suggest that the M2 segment forms the majority of the lining of the channel and is largely α-helical. This hypothesis is supported by the fact that synthetic peptides corresponding to the M2 segment self-assemble in bilayers to form cation-selective channels with properties resembling those of the nAChR itself (Oiki et al., 1988; Montal, 1995).

Cryoelectron microscopy (cryo-EM) experiments on 2D crystals of nAChRs from *Torpedo marmorata* have provided structures at 9 Å resolution of both the closed (Unwin, 1993, 1996) and open (Unwin, 1995) structures, which reveal the overall shape of the receptor and certain structural details. In particular, there are five kinked rods of density, one from each subunit, which appear to span the membrane and surround a central pore. This bundle of rods has been associated with the M2 helices. The kinks appear to be formed near the centers of the M2 helices, and it has been suggested (Changeux et al., 1992; Unwin, 1993) that leucine residues here form a hydrophobic barrier to ion permeation that gates the channel in the closed state. There is evidence in support of this (Revah et al., 1991; Labarca et al., 1995; Tierney et al., 1996), although other experiments have been interpreted in terms of a gate closer to the cytoplasmic end of the helices (Karlin and Akabas, 1995). In the open state the M2 helix bundle forms a right-handed supercoil; in the closed state it is weakly supercoiled in a left-handed fashion. The topology of the outer rim of the transmembrane region remains almost entirely unknown. Fourier transform infrared measurements of this region (obtained by cleaving off the extramembranous domains) suggest a mixed α/β structure (Hucho et al., 1994).

Candidate structures for the bundle of pore-lining M2 helices in both the closed and open states of the channel have been developed through the simulated annealing by restrained molecular dynamics (SA/MD) technique (Kerr et al., 1994; Sansom et al., 1995; Sankararamakrishnan et al., 1996). These structures were generated by using restraints derived from cryo-EM structures and are consistent with mutagenesis data. They were solvated with the TIP3P model of water (a three-center model) and studied by extensive molecular dynamics (MD) simulations. We have not included any transmembrane segments other than M2, given the ambiguity and paucity of the data concerning the secondary structure of these other segments. Although this means that our model of the pore lining is incomplete, data suggest that the M2 segments are the dominant elements in channel/ion interactions. Nevertheless, the simplicity of the

model system means that care must be taken when relating the results obtained here to a real nAChR, particularly to the heteropentameric $\alpha_2\beta\gamma\delta$ muscle nAChR.

The investigations can be conveniently divided into two parts. In the first part, the focus of examination is the water itself, and in particular the effects that its confinement within the M2 helix bundle has on its properties. We have also examined the hydrogen-bonding patterns of water and protein side chains in the pore, and the ability of the central ring of leucine residues to occlude the closed channel.

In the second part, a sodium ion is introduced into the pore of the open and closed channels. The ion is placed successively at a series of points along the length of the pore, and its z coordinate is restrained throughout a short MD simulation. The energetics of the ion's interaction with the water and protein side chains, and its perturbation of the orientation of the water in its neighborhood, are investigated. From this comparatively simple approach, we attempt to make qualitative explanations of selectivity and gating.

METHODS

M2 sequence

The system chosen for this investigation was a homopentameric bundle of the M2 segment of the α7 nAChR sequence from chick neuron:

```
-1' 0'  2'      6'     9' 10'  12'               20'
  E   K I S L G I T V L L  S  L  T  V F M L L V A  E
```

Note that we employ the same numbering scheme as that used by Lester (1992) and Labarca et al. (1995), whereby the first glutamate of M2 (corresponding to the "cytoplasmic intermediate ring" of acidic residues) is numbered $-1'$, and the last glutamate (corresponding to the "extracellular ring") is numbered 20'. This is a change from our earlier papers (Sankararamakrishnan and Sansom, 1994, 1995a–d; Sankararamakrishnan et al., 1996), where residue $-1'$ was numbered 1'. A homopentamer of α7 subunits is known to be able to form a functional channel, at least in vivo, and such α7 channels have been the subject of mutagenesis studies (Changeux et al., 1992; Galzi et al., 1992; Bertrand et al., 1993a,b). The use of a homopentamer constitutes a simplification of the model compared to the nAChR found in the nerve-muscle synapse, with its heteropentameric $\alpha_2\beta\gamma\delta$ stoichiometry. The leucine that is thought to occlude the pore in the closed conformation is L9', and the hydroxyl-containing residues that line the pore of the open channel in our model are S2', T6', and S10'. The N-terminus is blocked with an acetyl group and the C-terminus with an amino group, to approximate the effect of the preceding and following residues.

Channel models

All model generation and simulations were performed using Charmm23 (Brooks et al., 1983) on Silicon Graphics Indigo2 and DEC α workstations. The param19 force field (version 19 of the Charmm parameter set) was used. Only polar hydrogens were represented explicitly, and an extended-atom representation of nonpolar hydrogens was employed. Nonbonded interactions (van der Waals and electrostatic) were cut off at 14 Å with a switching function. Structures were visualized and analyzed with the aid of Quanta, Grasp (Nicolls et al., 1993), and MolScript (Kraulis, 1991).

Initial models of M2 helix bundles, in both an open and a closed conformation, were generated by restrained molecular dynamics simulations in vacuo, as described in previous papers (Kerr et al., 1994; Sansom

et al., 1995; Sankararamakrishnan et al., 1996). In these simulations, a combination of restraints was employed to generate ensembles of structures consistent with the cryo-EM data (Unwin, 1993, 1995) on the location of the M2 helices, and mutagenesis data on the identity of the pore-lining side chains (Akabas et al., 1992, 1994). The cryo-EM data were for the heteropentameric *Torpedo* nAChR, but as fivefold rotational averaging had been employed on the TM region of this structure, it was reasonable to apply it to the α7 nAChR. One structure was selected at random from each ensemble (open and closed) to serve as the starting point for the simulations described here.

Solvation and MD simulations

Each selected structure was solvated with the modified TIP3P water model of the param19 force field. The waters to be used were selected from a preequilibrated water box, first by cutting out an hourglass-like shape defined by the axes of the α-helix template, then by combining this with the protein of the M2 bundle and deleting those water molecules that approached protein atoms to within the sum of their van der Waals radii. The hourglass shape was extended ~10 Å past the end of the channel protein to define water "caps" to the model, mimicking the solvation of the mouths of the native channel, and providing a reservoir, allowing a measure of adjustment in the number of waters filling the channel. This procedure yielded solvated systems containing 1295 water molecules in the closed-channel model and 1027 in the open-channel model. The closed channel contains more water, primarily because the orientation of the helices in this configuration produces an "hourglass" with a steeper opening angle and thus larger water caps.

To prevent waters from escaping from the caps and from the channel through gaps between the helices, they were restrained throughout the simulation with an hourglass-shaped restraint imposed with a modified version of Charmm's mmfp module. These restraints were similar to those employed in MD studies of somewhat simpler channel/water systems (Breed et al., 1996). Following standard MD procedure, the models were energy-minimized, heated, and equilibrated before the simulation proper was begun. Minimization employed 3000 steps of the adapted-basis Newton-Raphson method. The minimized configurations thus produced were used to define the desired structure of the channel in the closed/open state, as appropriate. Thereafter, the integrity of the structures was maintained by harmonic restraints of 10 kcal mol^{-1} Å^{-2} on the backbone Cα atoms in residues $-1'$ to 6' and 11' to 20', keeping them close to their positions at the end of the minimization stage. In the absence of any other explicit protein, the artificial restraining potentials were essential to hold the M2 helix bundle in the desired configuration and to maintain the solvation water within the channel. Minimization was followed by 6 ps of heating, with the temperature increased by 5 K by velocity rescaling every 0.1 ps, to a final value of 300 K. Finally, 9 ps of equilibration at the final temperature of 300 K was performed, and the velocities were rescaled if the effective temperature fluctuated more than 10 K. The time step used in these and all subsequent MD simulations was 1 fs, with the length of all X-H bonds constrained by SHAKE.

The production stage of each simulation then followed, in which the average properties of the system were measured. For the open-channel model, this was 185 ps; the procedure in the case of the closed model was slightly more complex. The initial closed-state model was based on the assumption that the side chains of the L9' residues were close-packed, so as to occlude the pore. In the current simulations, we wished to examine whether such close packing would be found only if distance restraints were applied between the L9' side chains, and to examine the dynamic properties of closed-state models with and without such restraints. Thus distance restraints between the Cβ atoms of the L9' side chains, maintaining their close packing, were applied (for the closed-state model) during minimization/heating/equilibration and maintained for the first 185 ps of the simulation stage, to yield what will hereafter be referred to as the closed I trajectory. At $t = 185$ ps, the L9' restraints were removed, and the following 240 ps correspond to the closed II trajectory. Thus the closed I trajectory was 185 ps; the closed II was 240 ps, but only the last 185 ps was used to evaluate averages, to allow time for the structure to restabilize.
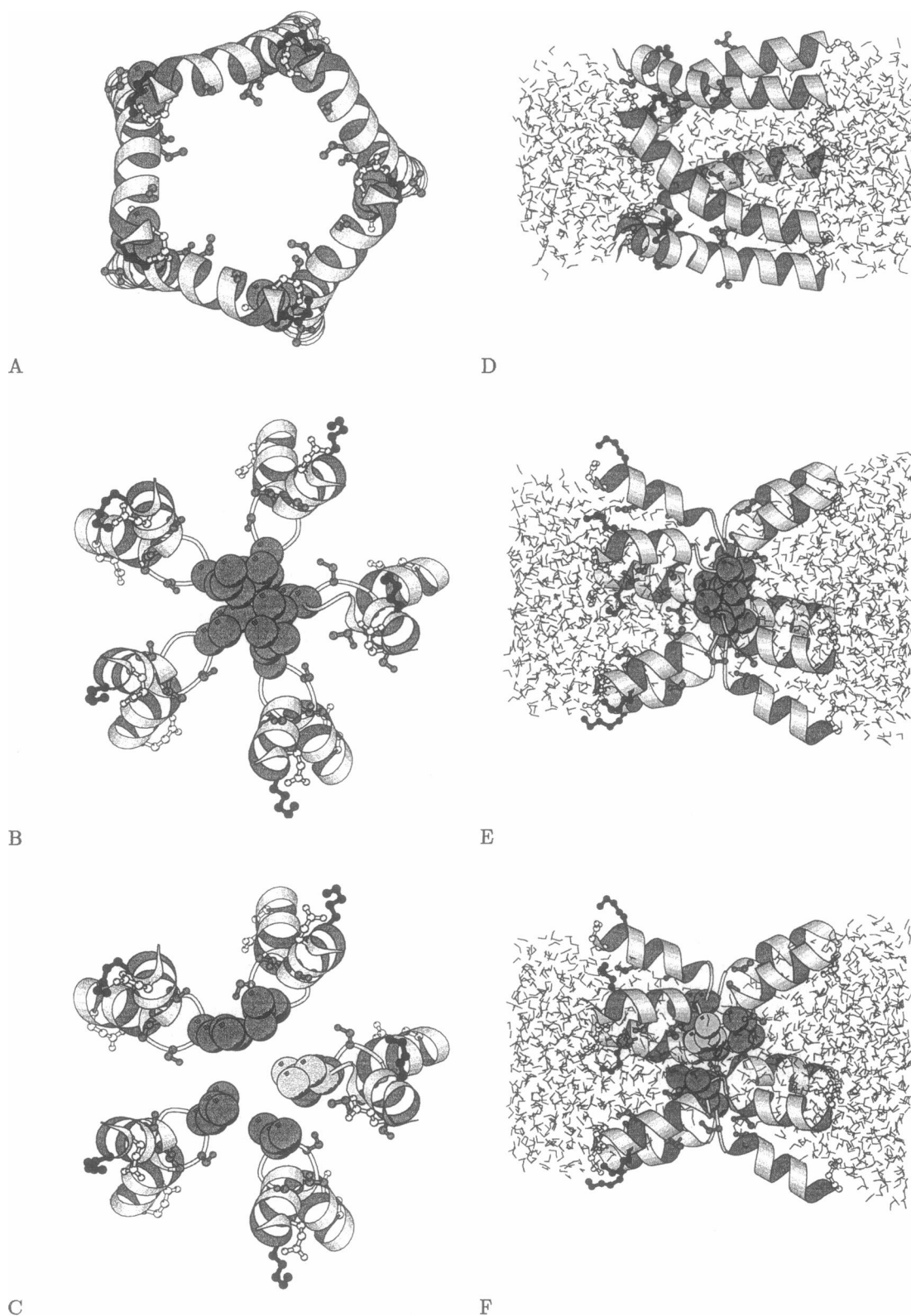
FIGURE 1 Molscript diagrams of the model channel in the open (*A*, *D*), closed I (*B*, *E*), and closed II (*C*, *F*) conformations, viewed down the transmembrane axis from the cytoplasmic (N-terminal) end in *A–C* and from the side in *D–F*. These structures all come from the ends of 185-ps MD trajectories. Positively charged side chains are shown in black, negatively charged in white, polar in mid-gray. The side chains of the L9' residues are shown as mid-gray van der Waals spheres, and the one L8' side chain that moves into a pore-lining conformation during the simulation is shown in light grey.

Typical configurations of all three models are shown in Fig. 1. These configurations come from the ends of the trajectories. The pore is clearly much more occluded by the L9' side chains in the closed I model than in the closed II model, and it can also be noted that there are differences in the backbone geometry in the channel center; this is discussed further below. A greater degree of exposure of the hydroxyl-containing side chains in the open channel is also apparent. Moreover, the helices splay out at the C-terminus of the open model, and at both termini of the closed models. It is therefore in these regions that the side chains of the M1 segments are likely to be exposed, and hence (even assuming that the models of M2 are correct) that the discrepancies between the model and the real receptor will be greatest.

Simulations with Na$^+$ ions

An ultimate goal of our studies of the pore region of the nAChR is to understand the molecular basis of the ionic selectivity, gating, and conductivity of the channel. As a first step toward this, we have conducted simulations in which a Na$^+$ ion is placed at 37 points along the axis of the pore, i.e., at $(0,0,z_i)$, $i = 1,37$ with a separation of 1 Å between the points. At each position of the ion, the system is energy-minimized through 3000 steps, heated to 300 K over 6 ps, and equilibrated for 9 ps. This 9 ps also serves as a short "production" stage from which the average interaction energies of the ion with the channel water and protein may be evaluated. Thus estimates of these interactions as functions of the z position of the ion are obtained. Although each simulation is short (15 ps in total), the total time expended is appreciable (500 ps for each channel model). The procedure is similar to that followed by Singh et al. (1996).

Each ion-containing structure was generated starting from the configuration of the appropriate solvated channel model from the end of the 185-ps trajectory. The ion was placed at the desired point of the channel axis, and to keep it near this position, its z coordinate was thereafter restrained with a harmonic potential with a force constant of 10 kcal mol^{-1} Å^{-2}. The nearest water molecule was removed to provide for easier relaxation of the water nearby. This structure was then minimized, heated, and equilibrated.

RESULTS

The geometry of the closed-channel models

The differences in geometry between the two closed channel models, I and II, resulting from the removal of the Cβ restraints, have been analyzed in some detail. The pore is clearly wider in the closed II model (Fig. 1, *B* and *C*), a finding confirmed by inspection of solvent-accessible surfaces (not shown). Furthermore, in the closed II model, the side chains that are nearest the pore axis are not exclusively those of the L9' residues. For example, in one of the M2 helices (referred to as P2 in our numbering scheme), an L8' residue occupies a position approximately equivalent to the L9' residues in the other helices (Fig. 1 *C*). Inspection of the trajectory shows how this comes to happen: interestingly, the L8' side chain of the P2 helix begins to move around to face the channel lumen ~150 ps into the closed I trajectory, i.e., before the Cβ restraints on L9' are removed. Thus both the L8' and L9' side chains of P2 are roughly equally exposed at 185 ps (when the L9' restraints are removed). A similar process happens to a much smaller extent in the other helices; their L8' side chains remain close to their initial positions, packed into the interfaces between the helices. After the Cβ restraints are removed, the L9' side

chains of all helices move away somewhat from their initial channel-occluding positions. In some helices this happens almost immediately; for the P2 helix it occurs only at ~240 ps. After this, it is the L8' side chain of P2 that is nearest to occupying the channel-occluding position. For the other helices, however, the L8' side chains are still only slightly exposed to the channel lumen.

A more detailed framework for the interpretation of these results is provided by the (ψ, ϕ) trajectories for both closed I and closed II models for the center-channel residues (7'-10') of the helices, labeled P1–P5. The key change, shown in Fig. 2 *A* for segment P1, is the relaxation of L9' from an initial β-like conformation to a final conformation that is more typical of an α-helix. This is seen in all five of the helices, although in the case of P2 it does not occur until 40 ps after the removal of the restraints. It is this, primarily, that moves the L9' side chain out of the center of the pore. Conversely, in helices P2 and P3 the L8' residue moves from an α to a β conformation (L8' in the other helices remains α-like). This transition begins to occur after ~120 ps, before the restraints are removed. The fact that the transition leads in only one case to the exposure of L8' to the pore is due to the conformation of V7': in helix P2, where L8' is finally exposed, V7' has a β-like conformation, whereas in the other helices it is α-like. This difference is found in the model from the beginning, having originated in the SA/MD process. Residue S10' also changes its configuration appreciably in helix P2, moving to much more typical α-helical values. The patterns of residue exposure implied by cysteine-scanning mutagenesis near the center of the closed channel do suggest a secondary structure that is irregular (Akabas et al., 1994), and moreover suggest that L8' is exposed to the pore. However, experiments on gating do not show a clear role for L8' in this (Revah et al., 1991; Labarca et al., 1995).

An analysis of the protein-protein hydrogen bonding in the various models has also been undertaken (protein-water hydrogen bonding is examined below), using the Charmm H-bonding potential to define the existence or absence of a H bond between two atoms: a bond is considered to exist if the D-H $\cdots$ A length is less than 4 Å and the D-H $\cdots$ A angle is less than 90°. In Fig. 2, *B–D*, the number of α-helical (i.e., $i \leftarrow i + 4$) H bonds formed in each of the three models is shown. In comparing the closed I and closed II models, it is apparent that the closed II model forms two strong $i \leftarrow i + 4$ hydrogen bonds in the central part of the helix (to residues 6' and 7'), and numerous partial H-bonds, whereas only one such bond is formed in the closed I model. In both closed models, however, the α-helical hydrogen bonding is much weaker than it is in the open model, because of the greater helix kinking: between 9 and 12 α-helical bonds per M2 helix are formed, compared to 15–17 in the open model. In some measure this is compensated for by the much larger number of $i \leftarrow i + 3$ and $i \leftarrow i + 5$ hydrogen bonds formed in the closed-channel models (data not shown), but overall the greater number of protein-protein H-bonds is formed in the open model: 28 ± 2.5 per

A

B

C

D
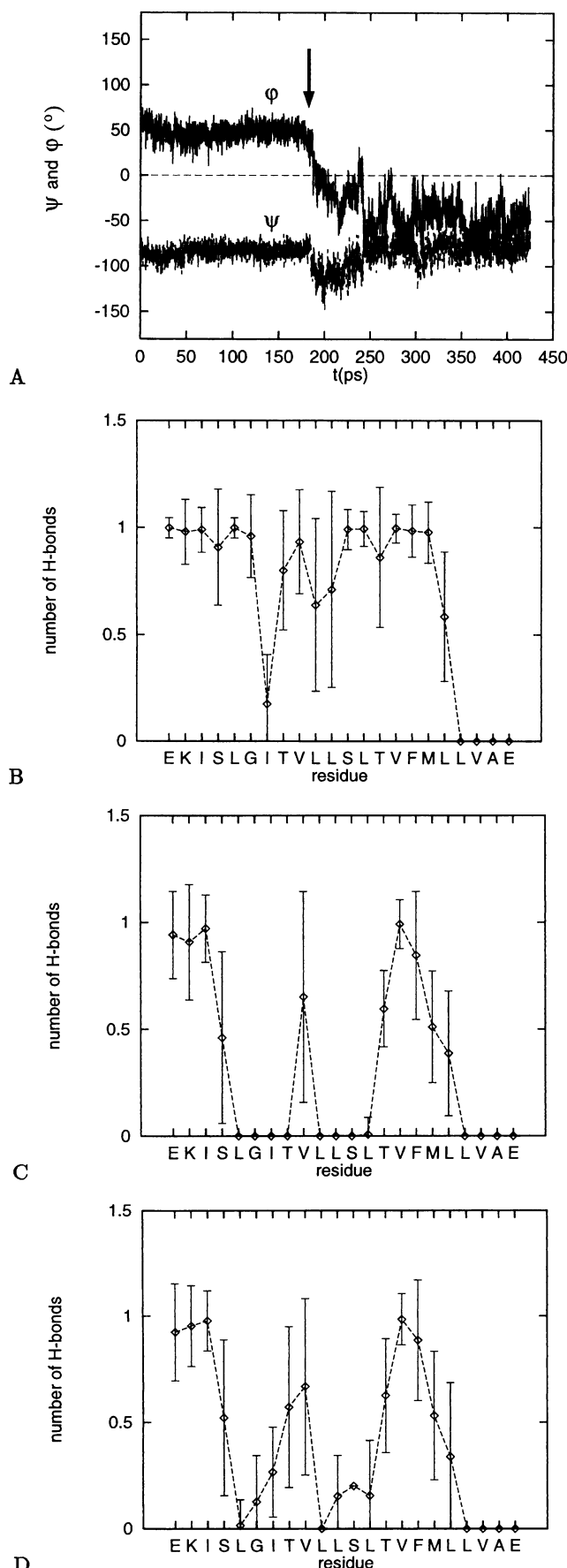
M2 helix compared to 23 ± 2.5 in the closed I and 22.5 ± 2 in the closed II models. It is interesting that, in the open model, the interruption of the helical H bonding at I5' (due to the kink at L9'; Fig. 2 B) corresponds to a H bond that lasts the length of the simulation. This H bond is formed between the backbone carbonyl of I5' and the NH_3^+ group of K0' of the next helix along, thus linking adjacent helices. Another protein-protein H bond that lasts throughout the simulation is that between the charged groups of K0' and E-1' (this, of course, could also be described as a salt bridge). The ends of the side chains of these two groups remain in close contact in all five helices of the open model, and in four of the five in the closed models.

Water dynamics

The dynamic behavior of the water molecules was characterized by the self-diffusion coefficient D (which measures translational mobility), and the rotational reorientation rate τ_1^{-1}, calculated from the mean squared displacement and the rotational correlation function as discussed by Breed et al. (1996). The dynamics of the water molecules in the simulation are thus summarized in Fig. 3, which shows D and τ_1^{-1} as functions of position z along the axis of the system. It should be noted that there is a clear reduction of the mobility of the water within the channel pore. In the open model, all of these measures of mobility are reduced to about one-third of their values in the "caps," which approximate the bulk water phase, whereas in the closed models there is about an order of magnitude reduction around $z = 0$, where the channel is narrowest. Similar reduction in mobility has been seen in many different systems, from simple nonatomistic models of hydrophobic channel-like cavities (Sansom et al., 1996b) to atomistic models of a number of different channels (Breed et al., 1996; Roux and Karplus, 1994; Engels et al., 1995; Chiu et al., 1996; Singh et al., 1996). The behavior of these measures of mobility in fact correlates very well with a simple measure of the channel radius, the number density of water molecules as a function of z. The highest values of D and τ_1^{-1} themselves, obtained in the centers of the cap region, are in good agreement with the values of $D = 0.32$ Å^2 ps^{-1} and $\tau_1^{-1} = 0.30$ ps^{-1} from a control simulation of 231 of the modified TIP3P waters, with periodic boundary conditions to mimic the bulk state (Breed et al., 1996). For comparison, the experimental values are $D = 0.23$ Å^2 ps^{-1} and $\tau_1^{-1} = 0.21$ ps^{-1} (Eisenberg and Kauzmann, 1969), although we consider the qualitative behavior of D and τ_1^{-1} through the

FIGURE 2   (A) Trajectories of backbone torsion angles ψ and ϕ of the closed I and closed II models for residue 9' in segment P1. The Cβ restraints are removed after 185 ps (arrow). (B–D) Average number (± standard deviation) of α-helical (i.e., $i \leftarrow i + 4$) hydrogen bonds formed by each residue in the open (B), closed (C), and closed II (D) channels (the H bond is ascribed to the acceptor).
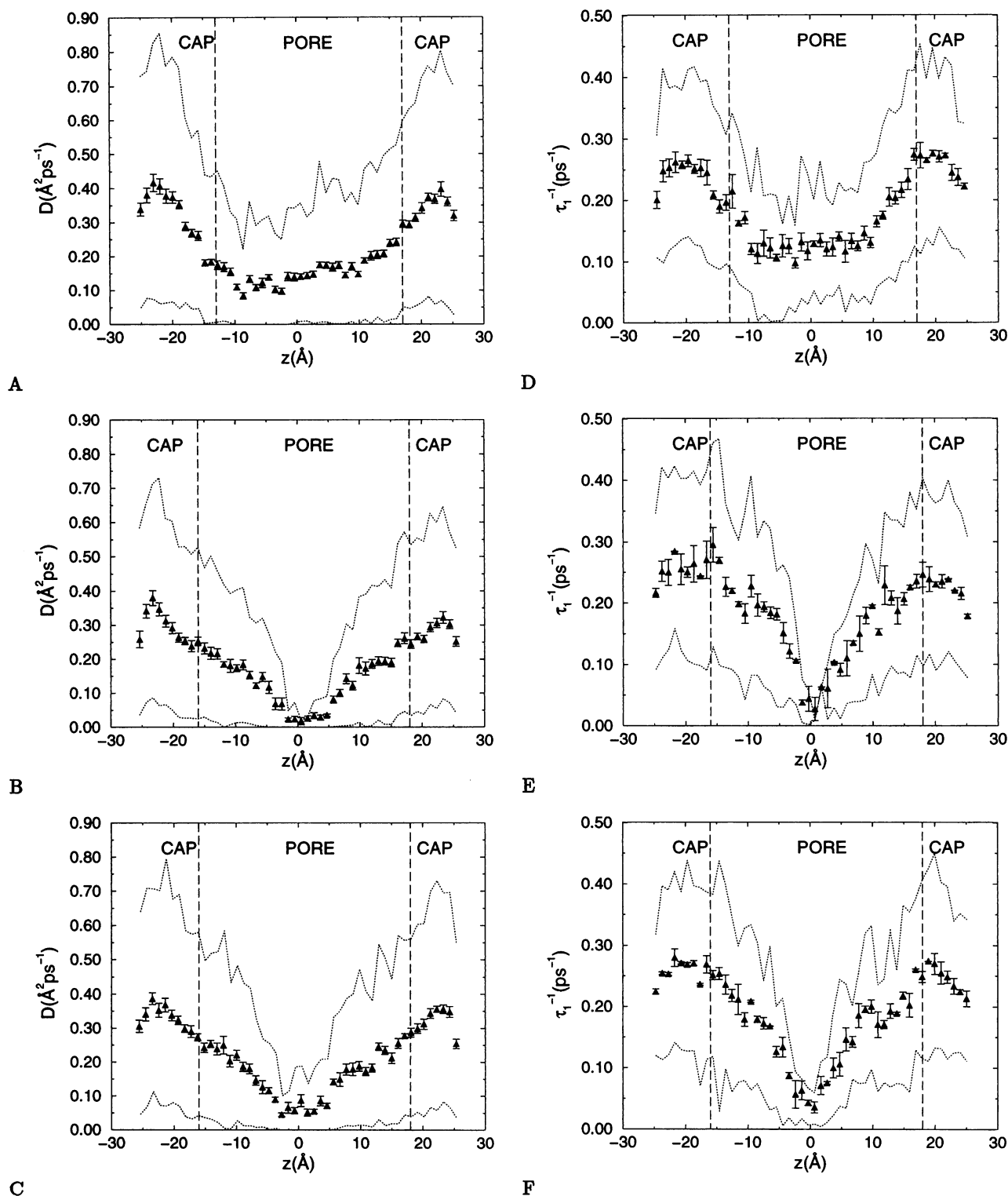
FIGURE 3 (A–C) Self-diffusion coefficient D as a function of average z position of water molecule in the open (A), closed I (B), and closed II (C) conformations. (D–F) Inverse rotational correlation time τ_1^{-1} as a function of average z position of water molecule in the open (D), closed I (E), and closed II (F) conformations. It should be noted that the error bars on these graphs are SEM errors; the magnitude of the typical variations found between individual water molecules is indicated by the dotted lines, which mark the 10th and 90th percentiles of the observed range of D and τ_1^{-1}.

channel pore to be of greater significance than this quantitative agreement.

Water and the L9′ gate

As has been remarked, it has been proposed (Changeux et al., 1992; Unwin, 1993) that the leucine residues at position 9′, which are thought to correspond to the apex of the helix kink, project into the channel in the closed state and are responsible for its gating, via hydrophobic interactions between the leucine side chains that lock them together, thus completely occluding the pore. Various experiments (Revah et al., 1991; Labarca et al., 1995; Tierney et al., 1996) have provided some measure of support for this. However, other gating mechanisms have also been proposed, involving, for example, a gate nearer the cytoplasmic end of the M2 helix or even in the loop between the M1 and M2 segments (Karlin and Akabas, 1995). The MD simulations allow us to examine the leucine-gate hypothesis in more detail, within the stated limitations of the model.

The local flux of water molecules within the channel is shown in Fig. 4. This shows the "gross" flux $J(z)$ (in molecules ps^{-1}) passing through a plane placed in the channel at z perpendicular to the pore axis. By "gross" flux we mean that molecules passing from left to right and from right to left are both counted with the same sign in $J(z)$; the numbers passing in the two directions are, in fact, equal, to within statistical errors, so there is no net flux, i.e., no net flow of water through the channel.

It is clear that the flux in the channel around $z = 0$ is somewhat reduced by the leucine ring in the closed II model; however, it is not much smaller than the lowest flux in the open channel, which occurs just inside the intracellular mouth, around $z = -8$, where the channel is narrow and is also appreciably occluded by the T6′ residues. Some experiments (Villarroel et al., 1991) implicate this as being the narrowest part of the channel, whereas others indicate the E-1′ ring (Wang and Imoto, 1992). For the flux through $z = 0$ to be appreciably smaller than that found in the open channel, it is necessary to go to the closed I model. Thus it appears that, without $C\beta$ restraints, the gate is some way from occluding the pore completely. This is confirmed by examination of sample trajectories of waters (data not shown); many water molecules succeed in passing across the "closed" gate, and some escape from the gate region on one side, having entered it from the other. The total displacements of these water molecules over the entire simulation time are no less than those of similar molecules in the open channel.

Water structure

The behavior of the water in the channel can usefully be described in terms of static, "structural" properties, in addition to the dynamic properties considered above. The first of these, the projection of the water dipole moments onto
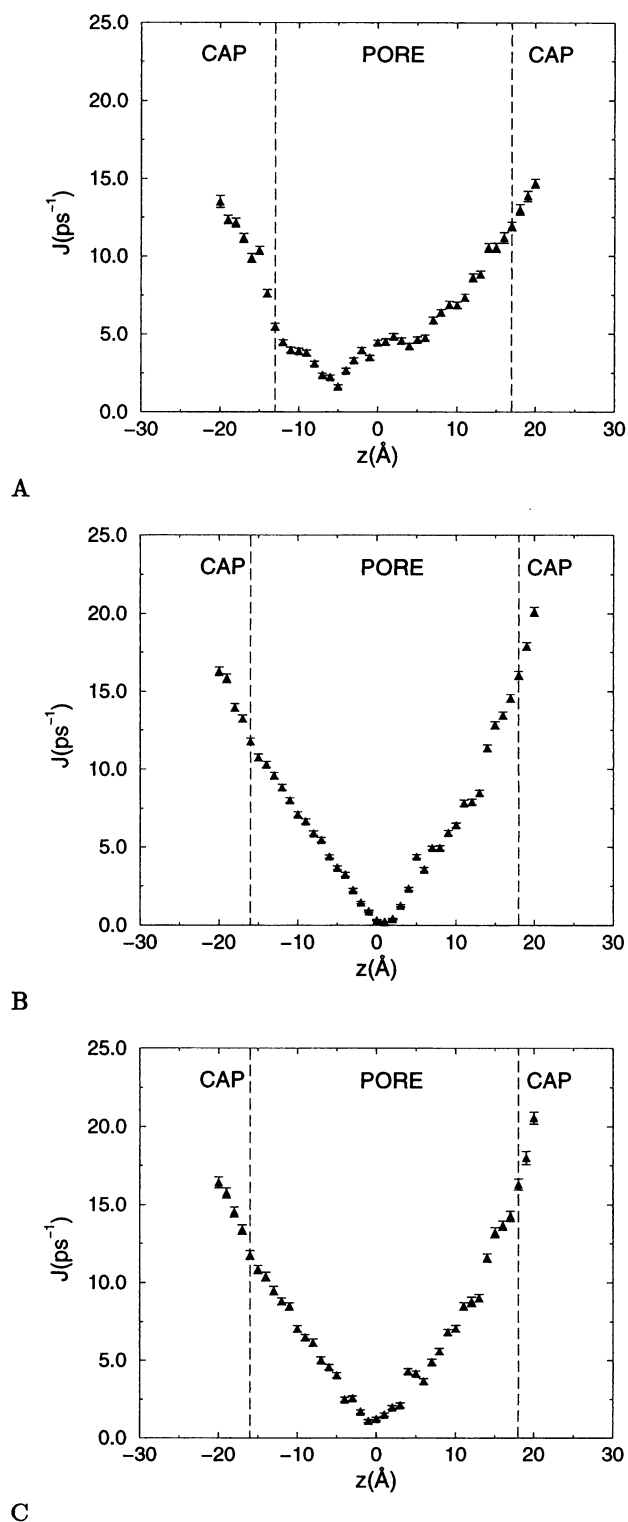

FIGURE 4   Gross flux of water J (i.e., molecules passing from left to right and from right to left are both counted with the same sign) through the channel in the open (A), closed I (B), and closed II (C) conformations.

the z axis, is shown in Fig. 5. For both open and closed channels, there is a clear tendency of the water molecules within the channels to align such that their dipoles are
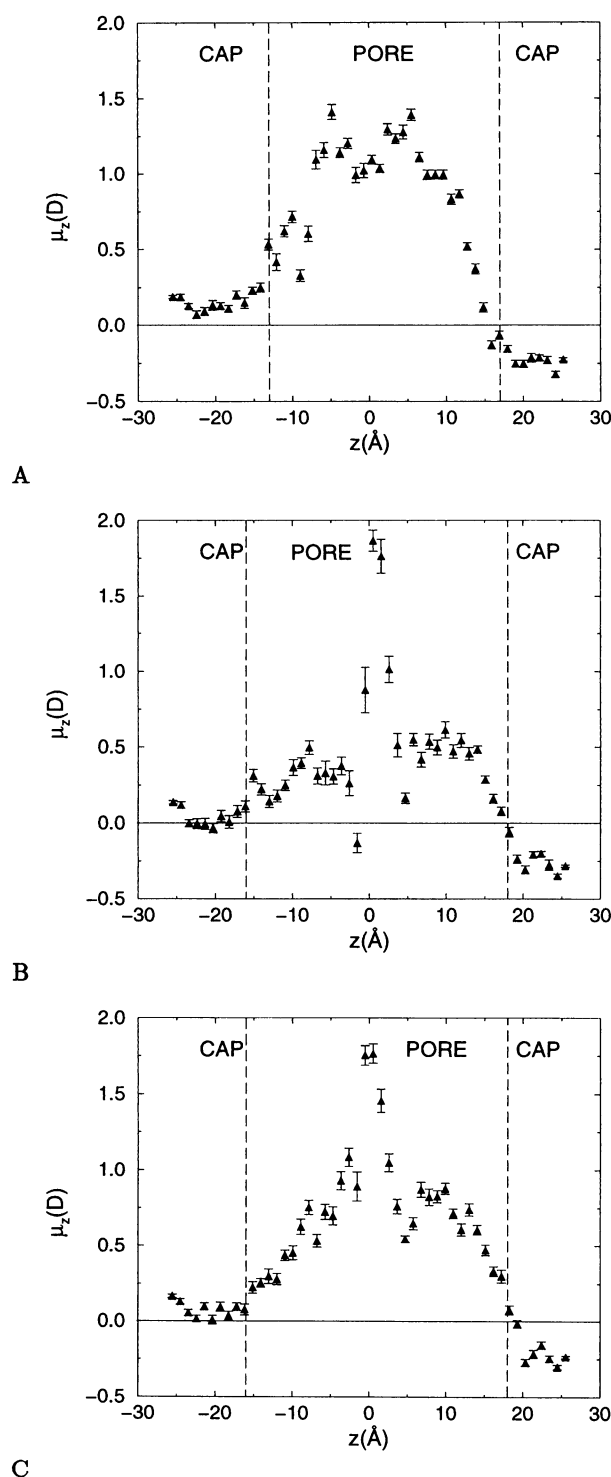
A

B

C

FIGURE 5   Average water dipole moment μ_z as a function of average z position of water molecule in the open (A), closed I (B), and closed II (C) conformations. A positive μ_z means that the water's hydrogen atoms have a greater average z coodinate than its oxygen.

antiparallel to those of the α-helix dipoles, as has already been seen in simulations of hydrophobic (Breed et al., 1996) and amphipathic (Sansom et al., 1996a; Mitton and Sansom, 1997) helix bundles. The water dipole thus points from the

cytoplasm into the extracellular medium. The greatest magnitude of the water's alignment, $\mu_z \approx 1.35$ D, is just over half of the total water dipole moment ($|\mu| = 2.35$ D for TIP3 water). Out of the channel pore itself, in the water "caps," the orientation of the water is much weaker but has the sign that would be expected if it were the field of the two rings of negative glutamates that were the predominant influence.

Consideration of channel water orientation leads naturally to consideration of orientations of side-chain OH groups. The results are summarized in Table 1. It is found that S2′, T6′, and T12′ are all oriented parallel to the helix dipoles, quite strongly in most cases. Although this may be expected to have some energetic cost, it will be partially offset by favorable dipole-dipole interactions with the channel waters, which, as we have seen, tend to have the opposite orientation. More important than this in the case of T6′ and T12′ will be hydrogen bonding back to carbonyls on N-terminally located residues, especially for T12′ in the open model, where it is unhydrated. However, there can be no such reason for the orientation of S2′, which forms H bonds only to water. It seems to be oriented as it is, mainly because a rotation about the Cα-Cβ bond, to produce a negative dipole moment, would take the hydroxyl into the channel, where it would cause steric interference with T6′ (the S2′ hydroxyl has, in fact, the most negative average z coordinate of any side chain in the open-channel model; i.e., it provides part of the cytoplasmic mouth of the open pore). In the open model S10′ has very little net dipole along the z axis ($\mu_z \approx 0.2$ D); in both closed models, however, it is oriented strongly antiparallel to the helix dipoles, mainly because of a strong H bond to the carbonyl group of L9′.

Another quantity of interest is local number and number density profiles of the channel water within the pore. The most natural way to consider this is to make a three-dimensional histogram $N(x, y, z)$ of the positions of water molecules, as defined by the positions of the water oxygen atoms, averaged over the various coordinate sets of the trajectory. Then a measure of "local density" is $n(x, y, z) = N(x, y, z)/\Delta x\, \Delta y\, \Delta z$, where the denominator corrects for the volume of the "bins" used in calculating the histogram.

TABLE 1   Dipole moments of hydroxyl-containing side chains

Residue	Model	μ_z (D)	H bonds to protein
S2′	Open	−1.13	None
	Closed I	−0.42	None
	Closed II	−0.36	None
T6′	Open	−0.74	S2′ C=O
	Closed I	−0.51	L3′ C=O
	Closed II	−0.56	L3′ C=O
S10′	Open	+0.21	None
	Closed I	+1.03	L9′ C=O
	Closed II	+1.40	L9′ C=O
T12′	Open*	−0.55	L8′ C=O
	Closed I	−0.15	V7′ C=O (weak)
	Closed II	−0.57	V7′ C=O (weak)

*Note that T12′ is not a pore-lining residue in the open model and thus is not hydrated in these simulations.

Thus $\int\int\int n(x, y, z)dx\,dy\,dz = N_v$, where N_v is the number of water molecules in the simulation volume V. In bulk water, where there is no permanent local structure relative to space-fixed coordinates, it follows from the density that $\langle n(x, y, z)\rangle = 0.03\ \text{Å}^{-3}$. $n(x, y, z)$ has been calculated for the nAChR models (using $\Delta x = \Delta y = \Delta z = 1\ \text{Å}$), and contour maps for constant-z slices in the open channel are shown in Fig. 6, A–C. These figures show $n(x, y, z)$ around the T6′ residues at $z = -7$, and they clearly show the substantial immobilization of channel water around these residues (the bottom contour, at $n = 0.1$, represents three times the bulk average). This level of immobilization is the highest that is seen in the pore lumen itself; the still higher peak of n further out shows water that has passed out of the pore into stable hydrogen-bonded "pockets" near lysine residues. We shall discuss both of these effects further when considering hydrogen bonding explicitly in the next section.

Similar peaks in $n(x, y, z)$, associated with waters lying close to the protein surface, are also visible elsewhere in the open channel and in the two closed models, although usually without the pleasing symmetry seen in Fig. 6, A–C. Immobilization near charged residues is seen, but also around the helix kinks and near polar backbone groups.

Aside from the fluctuation in local density caused by hydrogen bonding, there are also much smaller fluctuations (less than $\sim\frac{1}{2}\langle n\rangle$), which persist even in the center of the channel, away from the protein. We attribute these simply to the confining effect of the channel, as they are similar in magnitude and "wavelength" (~ 3 Å) to those seen in simulations of water within cylindrical hydrophobic cylinders (Lynden-Bell and Rasaiah, 1996). They are most clearly displayed above the "noise" by converting to cylindrical polar (r, θ, z) coordinates and averaging over θ, thus obtaining $n(r, z)$ (results not shown).

Hydrogen bonding

An investigation has been made of hydrogen-bonding networks between protein and water in the various channel models, relating in particular to the partially immobilized waters detected in the measurements of $n(x, y, z)$, which may alter the effective radius of the channel and thus affect the conductance properties. The hydrogen bonds were characterized as described in the section on channel conformation. The average number of protein-water hydrogen bonds is 132(7) in the whole of the open channel, 170(6) in the closed I channel, and 175(7) in the closed II. The greater number of bonds to water in the closed state reflects the looser packing of the helices, and it should be recalled that in the open state more are formed between protein residues, so that roughly the same total number of H bonds are formed in the three models.

In Fig. 7 we show the average number of water-protein H bonds formed by a particular residue, broken down into the contributions from the side-chain atoms (Fig. 7, A–C) and the peptide backbone (Fig. 7, D–F). Bonding to the side chains shows that about two H bonds are formed on average
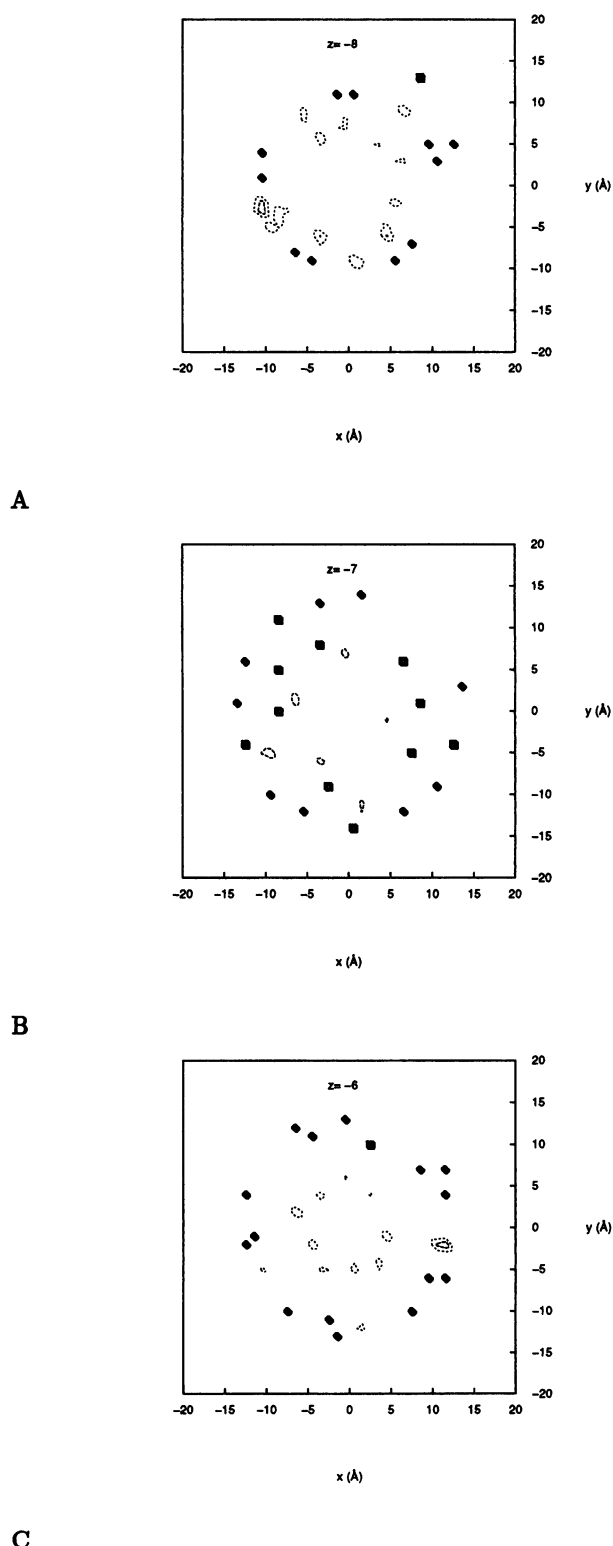

A

B

C

FIGURE 6   Local effective water density $n(x,y,z)$ in the open channel, for $z = -8$ Å (A), $z = -7$ Å (B), and $z = -6$ Å (C). The average positions of side chains are shown as black squares, and the average positions of backbone NH and CO groups as black diamonds. The bottom contour shows a density of 0.1 Å^{-3}; the next is at 0.25 Å^{-3}, and the next at 0.4 Å^{-3}.
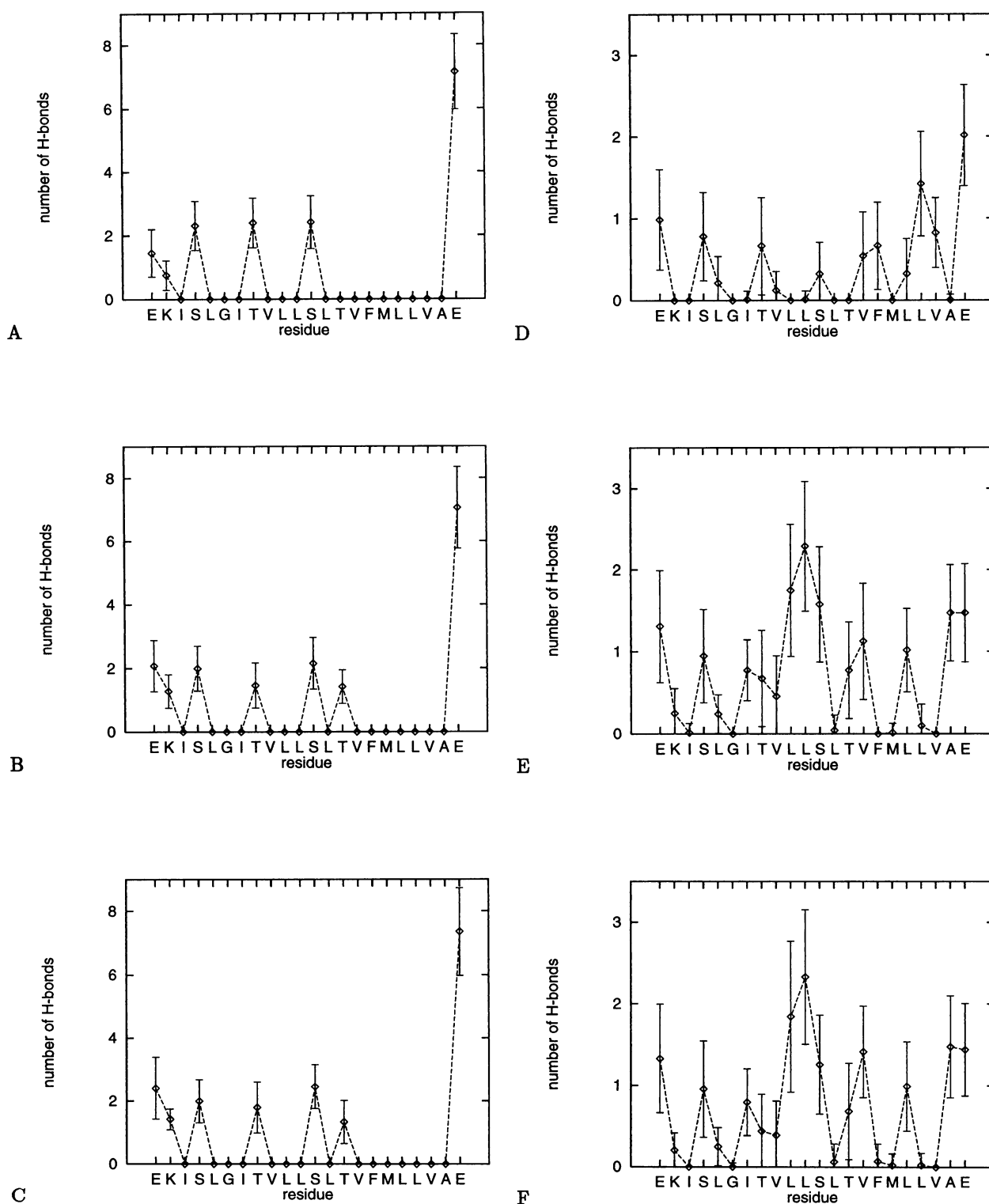
FIGURE 7 (*A–C*) Average number (± standard deviation) of hydrogen bonds formed per residue between water and protein side-chain atoms in the open (*A*), closed I (*B*), and closed II (*C*) conformations of the channel. (*D–F*) The same information for hydrogen bonds formed between water and protein backbone atoms.

by each of the polar residues, except for T12′ residues, which are not exposed in the open channel, and E20′, the glutamates of the extracellular ring, which are much more

heavily hydrated. However, this partially reflects the fact that they terminate the M2 fragments and so may be more exposed to solvent than they would be in the intact protein.

It also appears that S2' and T6' are rather more heavily hydrated in the open channel than in the closed, as expected, because the rotation of the M2 helices that accompanies the change from closed to open brings them more fully into the channel pore (see Fig. 1 and Sankararamakrishnan et al., 1996). The opposite is true of E-1' and K0'. Bonding to the backbone (Fig. 7, D–F) is limited in the open model and follows the expected pattern for an α-helix, increasing near the ends of the M2 segments, where the lumen opens up. It is very much more extensive in the closed models, reflecting the exposure of the backbone, particularly of residues L8', L9', and S10', near the kinks in the helices.

The average lifetime of these hydrogen bonds $\langle \tau \rangle$ has also been investigated, using the simple estimator $\langle \tau \rangle \approx \Delta t \langle n \rangle / N_T$, where Δt is the total length of the trajectory, $\langle n \rangle$ is the average number of water molecules that are H-bonded at any time, and N_T is the total number of different water molecules that form H bonds to the residue in question at some time during Δt. Commenting first on H bonds involving side chains: it is found that bonds to residues within the pore generally have longer lifetimes than those near the pore mouth, commensurate with the lower mobility of water in the pore. The fairly long lifetimes ($\langle \tau \rangle \approx 20$ ps) of H bonds to T6' and (to a slightly lesser extent) S10' in the open model are noteworthy, because they correlate with areas of high local density of water in the pore and so indicate a measure of local immobilization of water. We believe that this water might be sufficiently tightly bound to present a substantial free energy barrier to the passage of any permeant molecule large enough to have to displace them to pass. It could thus provide some measure of explanation of the fact that the minimum diameter of the open channel as estimated from blocking experiments with permeant ions (Dwyer et al., 1980; Villarroel et al., 1991; Wang and Imoto, 1992; Nutter and Adams, 1995) is appreciably less than that indicated by the structural information that informs the open model used here. Nevertheless, $\langle \tau \rangle$ is still less than 50 ps, and so these waters cannot be considered to be structurally bound. The most stably bound waters in the open channel are by far those that are found in pockets near K0' in the open channel, where at least one stable H-bonded network K0' $\cdots$ H$_2$O $\cdots$ T6' lasts throughout the simulation (185 ps). These waters show up as particularly high peaks of local density in Fig. 6 A. They are located outside of the channel pore, in the interfaces between helices. In the closed-channel models, the hydroxyl-containing side chains behave in a manner similar to that of the open model, but (unlike the open model) long-lasting H bonds ($\langle \tau \rangle \approx 20–40$ ps) are also formed between water and the exposed backbone of certain hydrophobic residues, notably V7', L8', L9', and V13', whereas H bonds with an average lifetime of 60 ps are formed with the peptide group of T12'.

Effect of Na$^+$ ions on water

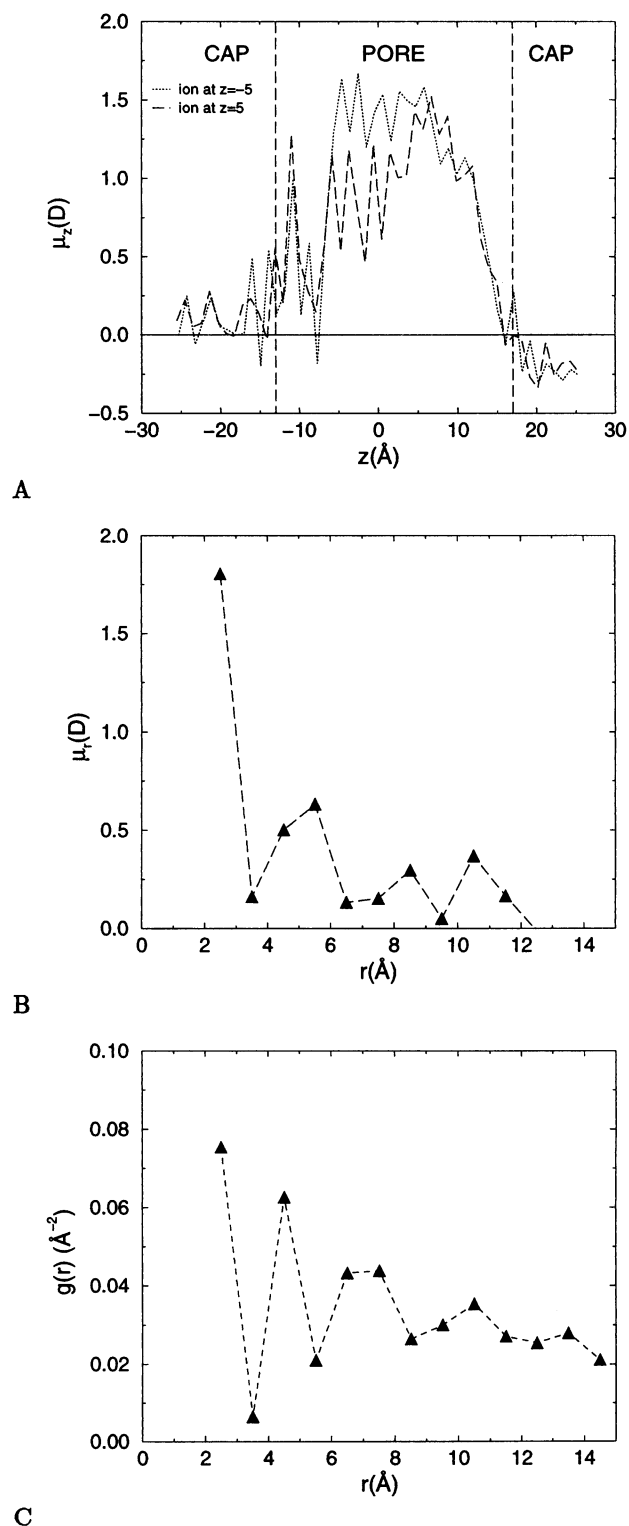We first investigate the effect that the ion has on the alignment of the channel water in the open channel. Fig. 8

A

B

C

FIGURE 8   (A) Average water dipole moment μ_z as a function of average z position of water molecule for two positions of the Na$^+$ ion in the open conformation. μ_z for the channel with no ion is shown for comparison. (B) Radial dipole moment of water $\mu_r(r)$. (C) Water-ion pair correlation function $g(r)$.

A shows μ_z for the water. If the ion alone were aligning the water, it would be expected to produce a μ_z that decreased from zero at large negative z to reach a minimum, then increased through zero (at the position of the ion) to a maximum, then slowly decreased to zero again. However, it is clear from Fig. 8 *A* that the ion has surprisingly little effect on the channel water (cf. Fig. 5 *A*). Indeed, given the comparatively large errors in these short calculations, it is hard to see any difference between μ_z with and without the ion that could be unequivocally attributed to its presence. Almost identical results were obtained in a control simulation in which the waters had no overall orientation before the addition of the sodium ion.

To see that the ion is indeed exerting a local influence on the water, it is necessary to measure $\mu_r = \langle \boldsymbol{\mu} \cdot (\mathbf{r_O} - \mathbf{r_{Na}}) \rangle$, the radial water dipole moment in a local coordinate system centered on the ion ($\mathbf{r_O}$ is the position vector of a water oxygen and $\mathbf{r_{Na}}$ that of the sodium ion). μ_r as function of $r = |\mathbf{r_O} - \mathbf{r_{Na}}|$ is shown in Fig. 8 *B*, together with the water-ion pair correlation function $g(r)$ (Fig. 8 *C*). Comparison of the dipole orientation with the local water density shows clearly the formation of a "hydration shell" of closest waters oriented with their oxygen atoms toward the ion, then a sparsely populated zone where waters are only weakly aligned (presumably oriented as much by the waters in the first hydration shell as by the ion itself), then a weak "second hydration shell."

Ion energy profiles

We have evaluated various energy terms, especially interaction energies involving the sodium ion, for the various positions of the ion in the three channel models, open, closed I (with L9' Cβ restraints), and closed II (without L9' Cβ restraints). It must first be remarked that, because the minimization and heating process is performed independently for each simulation, the total self-interaction energy of each system shows variations with the position of the ion which, while small on the scale of the total energy, are nevertheless O (100 kcal/mol), which is $\gg RT$ (and is on the same order as the ion's solvation energy, for example). Nor will the energies be a true $\langle U(T) \rangle$, as would be measured in a MC simulation, because, although the desired effective simulation temperature T is the same in all cases, it is defined only from the time average of the kinetic energy at the end of the heating stage, and so will not be identical for every position of the ion. These variations make it impossible to use the total energy as an indication of the existence of energetic barriers in the channel. Instead, specific interaction terms must be considered separately. In calculating such interaction energies, the range of the nonbonded interactions was increased to 20 Å, so that certain long-range interactions, such as the direct interaction between the ion and the glutamates, would not be cut off.

Considering first the interaction of the ion with all other parts of the system (Fig. 9), it is apparent in all three models
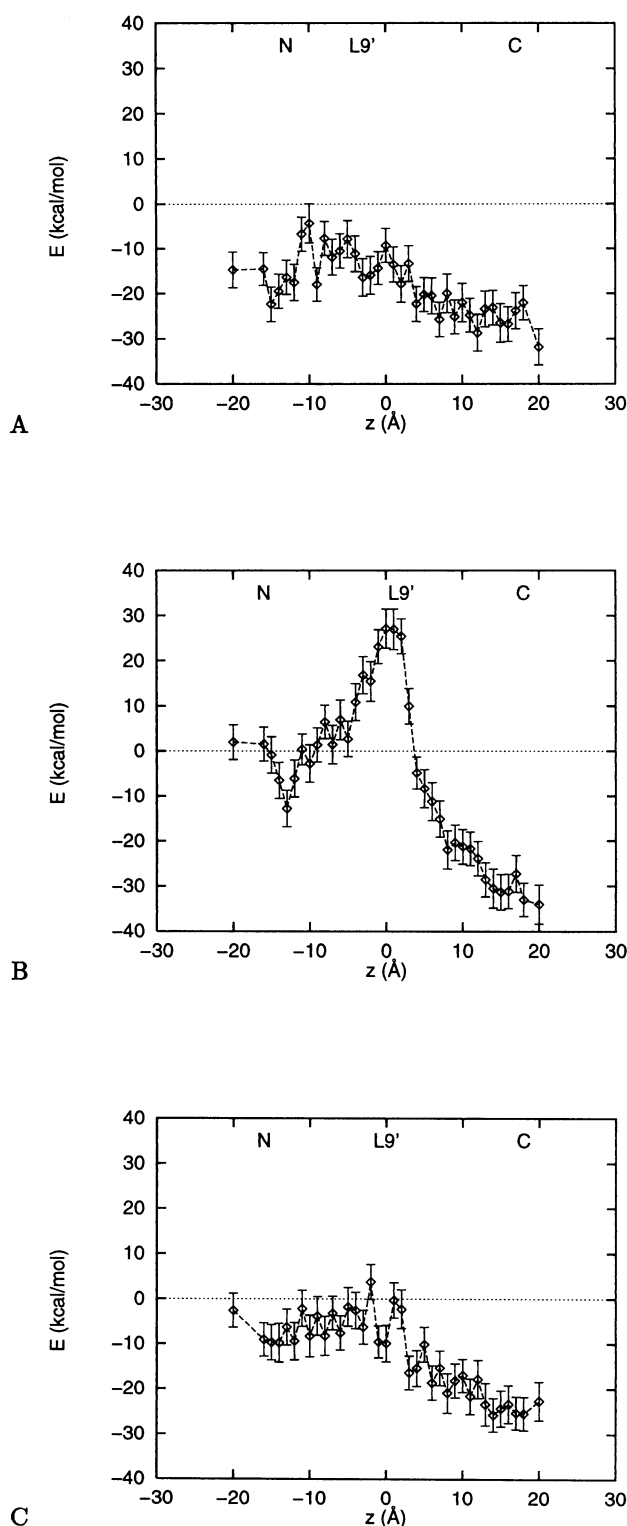

FIGURE 9 Total interaction energy between the ion and all other atoms as a function of z position of the ion for the open (*A*), closed I (*B*), and closed II (*C*) conformations of the channel. The interaction energies are calculated relative to the energy not of a bare ion but of a hydrated ion at infinity; this was estimated from a separate MD simulation of a sodium ion in a 46-Å³ cubic box of TIP3 water.

that there is an appreciable increase in energy on moving from the extracellular to the cytoplasmic side.

This reduction is due mainly to interaction with helix dipoles, and indeed the total ion-protein energy (Fig. 10,

A–C) shows a similar trend. However, few other features in the total energy are clear. The closed II model shows no clear barriers, confirming the findings for water alone, that the L9' residues do not clearly gate the channel, at least with the
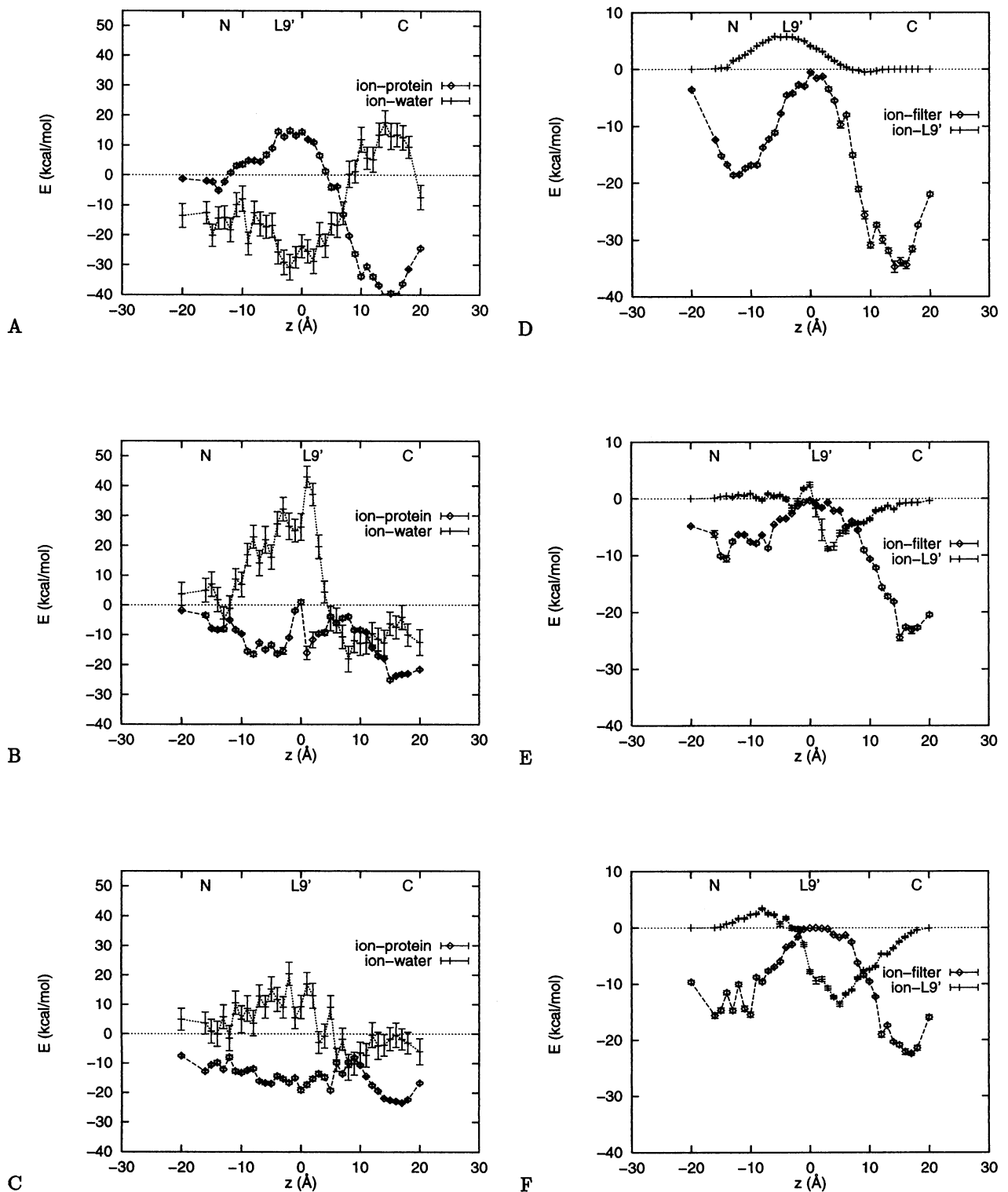

FIGURE 10   (A–C) Ion-protein and ion-water interaction energies as a function of z position of the ion for the open (A), closed I (B), and closed II (C) conformations of the channel. (D–F) The same information for ion-selectivity filter (E-1' + K0' + E20') and ion-L9' interaction energies. The ion-water energies are relative to zero for a hydrated, rather than a bare ion.

geometry of the model assumed here. The closed I model, however, does show a large barrier in the channel center.

Let us examine features of selectivity and gating in greater detail. The ion-selectivity filter (i.e., E-1' + K0' + E20') interaction energy (Fig. 10, *D–F*) shows the double-well structure expected for a permeating cation; at the cytoplasmic end, the negative glutamates comfortably outweigh the effect of the positive lysines. This energy is partially canceled by features in the ion-water energy (Fig. 10, *A–C*), as expected from the water's dielectric effect, but the double well remains just discernible in the total energy of the ion (Fig. 9). The interaction with the L9' residues (Fig. 10, *D–F*) is somewhat unexpected. In the open channel the interaction is moderately large and positive around the channel center; in the closed II channel, more importantly, it is S-shaped, with a much deeper attractive well than repulsive peak. Both of these features are due to interactions with the L9' backbone dipoles; the van der Waals energies are very small.

The presence of Cβ restraints is required before a direct barrier to ion permeation is produced (closed I model), and even then it is electrostatic in nature rather than coming from ion-protein van der Waals interactions (the L9' side chains are flexible enough, even with Cβ restraints, to move out of the way of the ion). Direct interaction with L9' is not, in any case, the main source of the observed maximum in the ion's total energy, even in the closed I model; most of it comes from the ion-water interaction energy (Fig. 10 *B*), which shows a clear maximum around $z = 0$ here, showing that appreciable dehydration of the ion is necessary before it can pass (a finding confirmed by examination of configurations of the system with the ion in this part of the channel). The ion-water interaction energy has a much smaller maximum in the closed II model, where the ion need not be so heavily dehydrated to pass, whereas in the open model the ion-water interaction energy, in fact, has a minimum in the channel center.

DISCUSSION

The validity of the models and methodology used

We shall now make a critical examination of the investigations that have been undertaken, commenting on the extent to which the approximations made in the model are likely to affect the validity of the results and, conversely, the extent to which deviations in the results from what would be expected in the light of experiment seem to call for modifications of the models.

Before embarking on a more detailed examination of the results, we make the general comment that the clearest deficiency of the present model is the absence of the outer TM segments of the protein and of the lipid. The lipid bilayer itself is probably far enough away from the M2 helices for its effect to be minimal (the distance is ≫ the Debye-Hückel screening length, ∼10 Å at physiological ion concentrations). Nearby protein from the other TM seg-

ments is likely to have a more important effect than lipid. As we have said, cysteine-scanning mutagenesis suggests that some protein of the M1 segment may be exposed to the pore in the open state (Karlin and Akabas, 1995), and indeed, in the models discussed here (particularly the closed models), there are gaps between the M2 helices that are probably closed by protein from other TM segments in the native receptor. This is therefore a good place to comment on alternative models of the channel that have been produced. One model is based on the known structure of heat-labile enterotoxin (Ortells and Lunt, 1996). This has α structure only for the M2 segments, which are similar to those in our model, although less strongly kinked. The rest of the TM protein consists of β-strands and turns. This is consistent with the findings of Fourier transform infrared experiments (Hucho et al., 1994), but there is little other evidence connecting the structure of the enterotoxin with that of the nAChR. A rather different model (not yet formulated at an atomic level) is that suggested by Karlin and Akabas from cysteine-scanning mutagenesis. In this model the M2 segment has a rather more irregular structure, especially in the open channel, and there is an appreciable contribution to the pore lining from the M1 segments. Moreover, motivated by the accessibility of mutated residues to extracellularly applied reagents in the open channel, they place the gate not at the center of the channel but at the cytoplasmic end, formed by the M1-M2 loop. However, at the present stage of knowledge of the structure of the receptor, it is very hard to be confident of the structure of any protein outside M2 and possibly parts of M1, and we prefer to omit this rather than include it in an arbitrary conformation. The structural effect of this protein in anchoring the ends of the M2 helices and (possibly) inducing their central kinks is instead captured by the use of restraining potentials on the positions of the Cα atoms, a technique that has been used elsewhere in the modeling of ion channels (Singh et al., 1996), while further restraining potentials approximate the effect of M1 in maintaining water within the pore. It is, of course, desirable that all pore-lining protein at least should be included, provided that there are grounds for believing this can be done accurately, and work on this is under way. We remark, however, that of the residues implicated by cysteine-scanning mutagenesis as pore-lining in the closed channel, none are charged and only one (an asparagine) is polar. Moreover, the pattern of exposure suggests a β-strand or irregular structure rather than an α-helix, and thus suggests that there will be no large net backbone dipole contribution. If this is true, the deficiencies in the model caused by the omission of M1 may not be too severe (the use of restraining potentials approximates far better to a uncharged, hydrophobic surface than to a charged or polar one).

Another possible source of error in our model might be the use of the cryo-EM data produced from the heteropentameric *Torpedo* nAChR to inform a model of a homopentameric $(\alpha 7)_5$ nAChR; recent studies (Kearney et al., 1996) have shown that the subunit-subunit interactions in the *Torpedo* nAChR do differ appreciably among themselves.

However, it is likely that the structures and interactions are similar enough to allow the the homologous residues in the two to play corresponding roles. Moreover, the EM density map in its present form is fivefold averaged and so probably corresponds more faithfully to the electron density of a homopentameric nAChR than it does to a $\alpha_2\beta\gamma\delta$ nAChR.

We also remark that, even though it is almost certain that some of the results presented here reflect inaccurate features of the model rather than the true behavior of water and ions in real ligand-gated channels, the techniques of analysis that have been developed will be immediately applicable to the improved models that will forthcoming with the improvement of the structural data.

At least regarding the coefficients D, μ_z, and τ_1^{-1} of the water, the findings here are likely to be robust under all but the most drastic modifications of the models. There is now a substantial accumulation of evidence from other studies (Breed et al., 1996; Sansom et al., 1996b; Roux and Karplus, 1994; Engels et al., 1995; Chiu et al., 1996; Singh et al., 1996) indicating that the observed reduction in D and τ_1^{-1} is a general feature of models where the molecules are constrained by lying within a pore, whereas the strong alignment of the water dipoles requires only that the channel should be formed by a parallel helix bundle (Breed et al., 1996).

Many of the features of the localization and hydrogen bonding of water molecules in the channel are also likely to be robust to changes in the model, because they probably depend only on the correct side chains being exposed correctly and the helix-bundle model being correct, to produce the strong overall E-field. Details of H bonding to backbone atoms are probably more model-dependent. The reduction in mobility by H bonding in the channel itself may, as we have said, reduce the maximum size of permeant organic cations and so relate to the fact that the apparent functional diameter of the channel is smaller than the electron microscopy data suggest, and so smaller than the diameter of the open model channel, as measured by the program HOLE (Smart et al., 1993; Sankararamakrishnan et al., 1996).

Permeation, gating, and selectivity

The measurements of water flux J provide information partially about the dynamics of water, but primarily about the center-channel geometry that is appropriate to the closed model, and to the extent to which the L9' ring gates the channel. This is also the primary significance of the conformational changes between the closed I and closed II models. It seems clear that in the model, the L9' ring is unable to prevent water permeation in the closed state without the presence of somewhat unphysical Cβ restraints. We are not aware of any experiments that show whether water can pass through the closed channel of the real nAChR.

It is perhaps unsurprising that hydrophobic interactions are not sufficient to close the channel entirely. The hydro-

phobic effect is not yet fully understood, but recent work from various sources suggests that the effective potential of mean force between two methane-sized cavities has an attractive well ~ 0.12 kcal/mol in depth (Smith and Haymet, 1993; Hummer et al., 1996; Lüdemann et al., 1996). We may therefore estimate the free energy of association of five leucines (~ 10 methyls) as being roughly 10 times this, giving an estimate of only $2RT$ at 300 K (this is, if anything, an overestimate, as overlaps between triplets will tend to reduce the total excluded volume). This estimate should be compared with the estimate of 1.4 kcal/mol ($\sim 2RT$) per leucine, from the effect of L9'S mutations on the apparent sensitivity to ACh (Labarca et al., 1995). Secondary structures that are known to be maintained by hydrophobic interactions seem to have a greater buried surface area than is found here, for example, the leucine zipper, in which at least 14 leucine residues come together. The above method leads in this case to an estimate of $6RT$ for the cohesive free energy.

The backbone conformational transitions that are observed around the center of the closed channel models should probably be interpreted as features of the present model only, because even fairly minor alterations to the model could change them appreciably. Most of the changes that occur serve to make the torsion angles more typical of an α-helix; this is particularly true of the L9' residues, which are initially in a β-like conformation. The exception is the $\alpha \rightarrow \beta$ transition of the L8' residue in one of the M2 helices, leading to exposure of its side chain. Because few experiments except cysteine-scanning mutagenesis have implicated L8' in lining the closed pore (Akabas et al., 1994), the most likely explanation is simply that in this respect the model differs from the real nAChR channel. However, it should be mentioned that L8' is extremely highly conserved (more so than L9' in fact), being present in every known nAChR sequence. The corresponding residue at position 8' in other related receptors is likewise absolutely conserved, although in the glycine and GABA$_A$ receptors it is a valine. This high conservation suggests that it plays some important role, which, if it is not in fact exposed, may thus be structural. In any event, the behavior of the simulation is consistent with the suggestion of Karlin and Akabas that the center of the M2 segment has an extended, irregular secondary structure in the closed state.

We now turn to a discussion of the investigation of ion permeation. This was only a preliminary investigation, and as such is capable of answering only some of the questions about the model. The short length of the simulation means that an estimate of only the internal energy of the ion is obtained, whereas it is the free energy of the ion that is really of interest. Differences between free energy and internal energy here would probably correspond to a difference in energy produced by the ion's finding lower energy states somewhere further off-axis, near a side chain, for example; the "pure" entropic term corresponding to the greater volume accessible near the ends of the channel is likely to be small compared to this. Thus the approximation

made is reasonable to the extent that the ion stays fairly near the axis of the channel, but there is little evidence either for or against this. Aside from this consideration, the independence of each simulation means that the total energy of the entire system cannot be used to give a clear measure of the stability of the structure with the ion at each point, as it could in a "true" constant-temperature simulation; random fluctuations in the energy obscure the signal, as was described above. It is necessary to concentrate on the ion's interaction energies, and doing so gives the expected qualitative behavior but ignores import interactions, such as the effect that the ion's presence has on the water-protein energy or the water's self-energy (these being an important part of the solvent's dielectric effect). The consequence of this is that the scale of the variation in the total system energy is likely in reality to be much smaller than the scale of the variation in the ion's total energy; indeed, the observed apparent potential barriers in the ion's total energy, typically on the order of 5 or 10 kcal/mol, would completely prevent permeation if reflected in the total free energy of the entire channel system in vivo. The short length of each simulation also produces large statistical uncertainties in the quantities measured.

That said, many qualitative features of the interactions studied would be expected to remain. The two rings of glutamate residues do produce potential wells (for a cation) at the mouths of the channel, that would attract a cation into the channel, and would repel an anion, thus providing justification for the hypothesis that these residues have a role in ionic selectivity. There are also slightly favorable interactions between the ions and the pore-lining hydroxyls such as T6', although the ion never moves far enough from the axis in our simulations to be coordinated directly by OH groups. Whether these interactions would differ in the case of anion permeation is not clear. There are certain energetic effects that have not been fully addressed here; for example, it is assumed that all E and K residues are in their fully ionized state. Continuum electrostatics calculations are under way (Adcock et al., unpublished results) to assess the validity of this assumption. They themselves might have to be modified in light of the alteration of the dielectric behavior of water in the channel that has already been alluded to. It is known that the opening of the nAChR is suppressed by a pH of less than 5 (Nutter and Adams, 1995), suggesting that some ionizable residues play a role, although whether these are in the pore-lining domains or elsewhere is at present unknown.

Another significant point is that there is a large increase in potential energy of the ion on passing through the channel from the extracellular (positive z in our model) to the cytoplasmic end (Fig. 9), mainly because of interactions with the helix dipoles. This effect is likely to be partially canceled by the neglected protein-water effects, and, in the channel in vivo, it would also be opposed by the resting membrane potential of about -60 mV ($q\Delta V \approx 1.5$ kcal/mol). However, these effects seem to be too small to cancel this protein-water energy entirely; it is probably valid to

conclude that the energy of our model system as a whole is also appreciably smaller when the ion is at the extracellular end. Because this is unlikely to be the case in the intact channel, it may be that inclusion of more of the channel protein will be required. The effective concentration of sodium within the channel in the conducting steady state may also be important in this respect.

The findings of the model are ambiguous with regard to the channel-gating mechanism as well. The results do not demonstrate that the proposed leucine-gating mechanism is correct, because the application of Cβ restraints was necessary to produce a clearly visible barrier; it appears that the hydrophobic effect is not strong enough between five leucines to produce the interdigitated barrier that is sometimes suggested to exist in the nAChR channel. On the other hand, the leucine-gating mechanism cannot be ruled out either, as it remains possible that sufficient gating is produced by the L9' ring; a energy difference of $\sim 5RT$ would be sufficient to gate the channel, but would not show up clearly in the measurements made here, because of the presence of noise. It is also possible that other features of the secondary structure (e.g., those resulting from the protein omitted in the present model or from a different spacing of the M2s) could help to maintain the cohesion of the L9' ring or could themselves contribute to the energetic barrier. The ability of water to flow across the gate in the closed II model is no more than suggestive of the possibility that ion permeation could also occur in the model, let alone in the real channel.

Conductance calculations: modifications of the open model

A major goal of our investigations of the nicotinic receptor is to be able to predict channel conductance. A direct measurement is beyond the computing power now available, and so indirect approaches must be used. The main components of a MD-based calculation of conductance (Roux and Karplus 1994; Roux et al., 1995) are a knowledge of the mobility (or, equivalently, diffusion coefficient) and the free energy of the ion as functions of z. Continuum approaches based on the Nernst-Planck equation (Levitt, 1991; Syganow and von Kitzing, 1995) or on even simpler models of effective conductance (Smart et al., 1997) suggest that the results for ion current are less sensitive to the free energy of the ion than might be expected, because the conducting steady state is a nonequilibrium state with a higher concentration of ions in the channel and a higher shielding of the electrostatic potential. Nevertheless, it is hard to escape the conclusion that a refined model of the channel will be required before conductance can be quantitatively understood. As well as possible changes to M2, it will certainly be necessary to investigate the effect of the inclusion of at least some of the M1 protein. Of course, such features may become clearer as higher resolution cryo-EM images become available (Unwin, 1996). Moreover, knowl-

edge of the charge charge states of ionizable residues should be included, as should the membrane potential, and the treatment of long-range electrostatics should be improved.

The other major influence on the conductivity is the mobility of the ion in the pore. This has been treated in the past as equal to the mobility in bulk electrolyte, which is almost certainly inaccurate. A direct measurement of it, possibly including more than one ion in the channel, will also have to be made.

CONCLUSION

Investigations of the behavior of water and ions in models of the transmembrane region of the nAChR, built on the basis of the best available direct and indirect structural information, have been conducted. The behavior of the water is appreciably altered, in agreement with a growing body of evidence; it is aligned almost to the point of dielectric saturation by the helix dipoles, and the mobility is substantially reduced by its confinement. Some water molecules, particularly in "pockets" but also to a lesser extent in the pore itself, are appreciably immobilized by H bonding to polar and charged residues.

Certain features of ion permeation, such as the cation selectivity of the nAChR, are also explained at least qualitatively by the investigations that have been conducted of certain components of ionic energy in the model. However, although the model remains plausible in light of these measurements, they do suggest that some modifications may be required before the gating of the closed channel can be explained and before the energy profile of the ion as it passes along the pore is such that the observed conductivity can be quantitatively reproduced. It is our intention to extend these studies of water and ions (including potassium and chloride ions) in the channel into full potential-of-mean-force calculations, to try to make a connection with the experimentally observed selectivity and conductivity.

REFERENCES

Akabas, M. H., C. Kaufmann, P. Archdeacon, and A. Karlin. 1994. Identification of acetylcholine receptor channel-lining residues in the entire M2 segment of the α-subunit. *Neuron.* 13:919–927.

Akabas, M. H., D. A. Stauffer, M. Xu, and A. Karlin. 1992. Acetylcholine receptor channel structure probed in cysteine-substitution mutants. *Science.* 258:307–310.

Bertrand, D., J. L. Galzi, A. Devillers-Thiéry, S. Bertrand, and J. P. Changeux. 1993a. Stratification of the channel domain in neurotransmitter receptors. *Curr. Opin. Cell Biol.* 5:688–693.

Bertrand, D., J. L. Galzi, A. Devillers-Thiéry, S. Bertrand, and J. P. Changeux. 1993b. Mutations at two distinct sites within the channel domain M2 alter calcium permeability of neuronal alpha-7 nicotinic receptor. *Proc. Natl. Acad. Sci. USA.* 90:6971–6975.

Breed, J., R. Sankararamakrishnan, I. D. Kerr, and M. S. P. Sansom. 1996. Molecular dynamics simulations of water within models of ion channels. *Biophys. J.* 70:1643–1661.

Brooks, B. R., R. E. Bruccoleri, B. D. Olafson, D. J. States, S. Swaminathan, and M. Karplus. 1983. CHARMM: a program for macromolecular energy, minimisation, and dynamics calculations. *J. Comp. Chem.* 4:187–217.

Changeux, J. P., J. I. Galzi, A. Devillers-Thiéry, and D. Bertrand. 1992. The functional architecture of the acetylcholine nicotinic receptor explored by affinity labelling and site-directed mutagenesis. *Q. Rev. Biophys.* 25:395–432.

Charnet, P., C. Labarca, R. J. Leonard, N. J. Vogelaar, L. Czyzyk, A. Gouin, N. Davidson, and H. A. Lester. 1990. An open-channel blocker interacts with adjacent turns of a-helices in the nicotinic acetylcholine receptor. *Neuron.* 2:87–95.

Chiu, S. W., S. Subramaniam, and E. Jacobsson. 1996. Simulation of a gramicidin channel in a fluid-phase DMPC bilayer. *Biophys. J.* 70: SU275.

Cohen, B. N., C. Labarca, L. Czyzyk, N. Davidson, and H. A. Lester. 1992. $Tris^+/Na^+$ permeability ratios of nicotinic acetylcholine receptors are reduced by mutations near the intracellular end of the M2 region. *J. Gen. Physiol.* 99:545–572.

Dwyer, T. M., D. J. Adams, and B. Hille. 1980. The permeability of the endplate channel to organic cations in frog muscle. *J. Gen. Physiol.* 75:469–492.

Eisenberg, D., and W. Kauzmann. 1969. The Structure and Properties of Water. Oxford University Press, Oxford.

Engels, M., D. Bashford, and M. R. Ghadiri. 1995. Structure and dynamics of self-assembling peptide nanotubes and the channel-mediated water organization and self-diffusion. A molecular dynamics study. *J. Am. Chem. Soc.* 117:9151–9158.

Galzi, J., A. Devillers-Thiery, N. Hussy, S. Bertrand, J. P. Changuex, and D. Bertrand. 1992. Mutations in the channel domain of a neuronal nicotinic receptor convert ion selectivity from cationic to anionic. *Nature.* 359:500–505.

Giraudat, J., M. Dennis, T. Heidmann, P. Y. Haumont, F. Lederer, and J. P. Changeux. 1987. Structure of the high-affinity binding site for noncompetitive blockers of the acetylcholine receptor: [³H]chlorpromazine labels homologous residues in the β chain and δ chain. *Biochemistry.* 26:2410–2418.

Hucho, F., U. Görne-Tschelokow, and A. Strecker. 1994. Beta-structure in the membrane-spanning part of the nicotinic acetylcholine receptor (or how helical are transmembrane helices?). *Trends Biochem. Sci.* 19: 383–387.

Hucho, F., and R. Hilgenfeld. 1989. The selectivity filter of a ligand-gated ion channel The helix-M2 model of the ion channel of the nicotinic acetylcholine receptor. *FEBS Lett.* 257:17–23.

Hucho, F., W. Oberthür, and F. Lottspeich. 1986. The ion channel of the nicotinic acetylcholine receptor is formed by the homologous helices M II of the receptor subunits. *FEBS Lett.* 205:137–142.

Hucho, F., V. Tsetlin, and J. Machold. 1996. The emerging three-dimensional structure of a receptor: the nicotinic acetylcholine receptor. *Eur. J. Biochem.* 239:539–557.

Hummer, G., S. Garde, A. E. García, A. Pohorille, and L. R. Pratt. 1996. An information theory model of hydrophobic interactions. *Proc. Natl. Acad. Sci. USA.* 93:8951–8955.

Imoto, K., C. Busch, B. Sakmann, M. Mishina, T. Konno, J. Nakai, H. Buyo, Y. Mori, K. Kukuda, and S. Numa. 1988. Rings of negatively charged amino acids determine the acetylcholine receptor channel conductance. *Nature.* 335:645–648.

Karlin, A., and M. H. Akabas. 1995. Towards a structural basis for the function of nicotinic acetylcholine receptors and their cousins. *Neuron.* 15:1231–1244.

Kearney, P. C, H. Zhang, W. Zhong, D. A. Dougherty, and H. A. Lester, 1996. Determinants of nicotinic receptor gating in natural and unnatural side chain structures at the M2 9' position. *Neuron.* 17:1221–1229.

Kerr, I. D., R. Sankararamakrishnan, O. S. Smart, and M. S. P. Sansom. 1994. Parallel helix bundles and ion channels: molecular modelling via simulated annealing and restrained molecular dynamics. *Biophys. J.* 67:1501–1515.

Kraulis, P. J. 1991. MOLSCRIPT: a program to produce both detailed and schematic plots of protein structures. *J. Appl. Crystallogr.* 24:946–950.

Kuyucak, S., and S. H. Chung. 1994. Temperature dependence of conductivity in electrolyte solutions and ionic channels of biological membranes. *Biophys. Chem.* 52:15–24.

Labarca, C., M. W. Nowak, H. Zhang, L. Tang, P. Desphande, and H. A. Lester. 1995. Channel gating governed symmetrically by conserved leucine residues in the M2 domain of nicotinic receptors. *Nature.* 376:514–516.

Leonard, R. J., C. G. Labarca, P. Charnet, N. Davidson, and H. A. Lester. 1988. Evidence that the M2 membrane-spanning region lines the ion channel pore of the nicotinic receptor. *Science.* 242:1578–1581 .

Lester, H. 1992. The permeation pathway of neurotransmitter-gated ion channels. *Annu. Rev. Biophys. Biomol. Struct.* 21:267–292.

Levitt, D. G. 1991. General continuum theory for multiion channel. I. Theory. *Biophys. J.* 59:271–277.

Lüdemann, S., H. Schreiber, R. Abseher, and O. Steinhauser. 1996. The influence of temperature on pairwise hydrophobic interactions of methane-like particles: a molecular dynamics study of free energy. *J. Chem. Phys.* 104:286–295.

Lynden-Bell, R. M., and J. C. Rasaiah. 1996. Mobility and solvation of ions in channels. *J. Chem. Phys.* 105:9266–9280.

Mitton, P., and M. S. P. Sansom. 1997. Molecular dynamics simulation of ion channels formed by bundles of amphipathic α-helical peptides. *Eur. Biophys. J.* 25:139–150.

Montal, M. 1995. Design of molecular function: channels of communication. *Annu. Rev. Biophys. Biomol. Struct* 24:31–57.

Nicholls, A., R. Bharadwaj, and B. Honig. 1993. GRASP: graphical representation and analysis of surface properties. *Biophys. J.* 64:166–170.

Nutter, T. J., and D. J. Adams. 1995. Monovalent and divalent cation permeability and block of neuronal nicotinic receptor channels in rat parasympathetic ganglia. *J. Gen. Physiol.* 105:701–723.

Oiki, S., W. Danho, V. Madison, and M. Montal. 1988. M2 delta, a candidate for the structure lining the ionic channel of the nicotinic cholinergic receptor. *Proc. Natl. Acad. Sci. USA.* 85:8703–8707.

Ortells, M. O., and G. G. Lunt. 1996. A mixed helix-beta-sheet model of the transmembrane region of the nicotinic acetylcholine receptor. *Protein Eng.* 9:51–59.

Revah, F., D. Bertrand, J. L. Galzi, A. Devillers-Thiery, C. Mulle, N. Hussy, S. Bertrand, M. Ballivet, and J. P. Changeux. 1991. Mutations in the channel domain alter desensitization of a neuronal nicotinic receptor. *Nature.* 353:846–849.

Role, L. W., and D. K. Berg. 1996. Nicotinic receptors in the development and modulation of CNS synapses. *Neuron.* 16:1077–1085.

Roux, B., and M. Karplus. 1994. Molecular dynamics simulations of the gramicidin channel. *Annu. Rev. Biophys. Biomol. Struct.* 23:731–761.

Roux, B., B. Prod'hom, and M. Karplus. 1995. Ion transport in the gramicidin channel: molecular dynamics study of single and double occupancy. *Biophys. J.* 68:876–892.

Sankararamakrishnan, R., C. Adcock, and M. S. P. Sansom. 1996. The pore domain of the nicotinic acetylcholine receptor—molecular modelling, pore dimensions and electrostatics. *Biophys. J.* 71:1659–1671.

Sankararamakrishnan, R., and M. S. P. Sansom. 1994. Kinked structures of isolated nicotinic receptor M2 helices: a molecular dynamics study. *Biopolymers.* 34:1647–1657.

Sankararamakrishnan, R., and M. S. P. Sansom. 1995a. Structural features of isolated M2 helices of nicotinic receptors: simulated annealing via molecular dynamics studies. *Biophys. Chem.* 55:215–230.

Sankararamakrishnan, R., and M. S. P. Sansom. 1995b. Water-mediated conformational transitions in the nicotinic receptor M2 helix bundles: a molecular dynamics study. *FEBS Lett.* 377:377–382.

Sankararamakrishnan, R., and M. S. P. Sansom. 1995c. Modelling packing interactions in parallel helix bundles: pentameric bundles of nicotinic receptor M2 helices. *Biochim. Biophys. Acta.* 1239:122–132.

Sankararamakrishnan, R., and M. S. P. Sansom. 1995d. Interaction of open channel blockers with nicotinic receptor channels—a molecular modelling study. *Biophys. J.* 68:A378.

Sansom, M. S. P., I. D. Kerr, P. C. Biggin, and P. A. Mitton. 1996a. Structure and dynamics of water within model transbilayer pores. *Biophys. J.* 70:A231.

Sansom, M. S. P., I. D. Kerr, J. Breed, and R. Sankararamakrishnan. 1996b. Water in channel-like cavities: structure and dynamics. *Biophys. J.* 70:693–702.

Sansom, M. S. P., R. Sankararamakrishnan, and I. D. Kerr. 1995. Modelling membrane proteins using structural restraints. *Nature Struct. Biol.* 2:624–631.

Singh, C., R. Sankararamakrishnan, S. Subramaniam, and E. Jakobsson. 1996. Solvation, water permeation and ionic selectivity of a putative model for the pore region of the voltage-gated sodium channel. *Biophys. J.* 71:2276–2288.

Smart, O. S., J. Breed, G. R. Smith, and M. S. P. Sansom. 1997. A novel method for structure-based prediction of ion channel conductance properties. *Biophys. J.* 72:1109–1126.

Smart, O. S., J. M. Goodfellow, and B. A. Wallace. 1993. The pore dimensions of gramicidin A. *Biophys. J.* 65:2455–2460.

Smith, D. E., and A. D. J. Haymet. 1993. Free energy, entropy and internal energy of hydrophobic interactions computer simulations. *J. Chem. Phys.* 98:6445–6454.

Stroud, R. M., M. P. McCarthy, and M. Shuster. 1990. Nicotinic acetylcholine receptor superfamily of ligand gated ion channels. *Biochemistry.* 29:11009–11023.

Syganow, A., and E. von Kitzing. 1995. Integral weak diffusion and diffusion aproximations applied to ion transport through biological ion channels. *J. Phys. Chem.* 99:12030–12040.

Tierney, M. L., B. Birnir, N. P. Pillai, J. D. Clements, S. M. Howitt, G. B. Cox, and P. W. Gage. 1996. Effects of mutating leucine to threonine in the M2 segment of a$_1$ and b$_1$ subunits of GABA$_A$ a$_1$b$_1$ receptors. *J. Membr. Biol.* 154:11–21.

Unwin, N. 1993. Nicotinic acetylcholine receptor at 9 Å resolution. *J. Mol. Biol.* 229:1101–1124.

Unwin, N. 1995. Acetylcholine receptor channel imaged in the open state. *Nature.* 373:37–43.

Unwin, N. 1996. Projection structure of the nicotinic acetylcholine receptor: distinct conformations of the α subunits. *J. Mol. Biol.* 257:586–596.

Villarroel, A., S. Herlitze, M. Koenen, and B. Sakmann. 1991. Location of a threonine residue in the α-subunit M2 transmembrane segment that determines the ion flow through the acetylcholine receptor channel. *Proc. R. Soc. Lond. B.* 243:69–74.

Wang, F., and K. Imoto. 1992. Pore size and negative charge as structural determinants of permeability in the Torpedo nicotinic acetylcholine receptor channel. *Proc. R. Soc. Lond. B.* 250:11–17.